Available online at www.sciencedirect.com

SciVerse ScienceDirect

Ceramics International 38 (2012) 6927–6930

CERAMICS INTERNATIONAL

www.elsevier.com/locate/ceramint

Short communication

Synthesis and Li electroactivity of $Fe_2P_2O_7$ microspheres composed of self-assembled nanorods

Gwang-Hee Lee, Seung-Deok Seo, Hyun-Woo Shim, Kyung-Soo Park, Dong-Wan Kim*

Department of Materials Science and Engineering, Ajou University, Woncheon-dong, San 5, Yeongtong-gu, Suwon 443–749, Republic of Korea

Received 28 April 2012; received in revised form 3 May 2012; accepted 11 May 2012
Available online 17 May 2012

Abstract

Iron phosphate ($Fe(II)_2P_2O_7$) microspheres composed of self-assembled nanorods were prepared by means of thermal dehydrogenation followed by thermochemical reduction of hydrothermally-synthesized $FePO_4 \cdot 2H_2O$ at 400 °C under a H_2 atmosphere. The phase and morphological evolutions of $FePO_4 \cdot 2H_2O$ and $Fe_2P_2O_7$ products were characterized by X-ray diffraction. The $Fe_2P_2O_7$ electrode as a new anode showed higher specific capacities (490 mA h g^{-1} after 10 cycles at a rate of 100 mA g^{-1}) and better cyclic performances than $FePO_4 \cdot 2H_2O$.

Keywords: E. Li-ion battery electrodes; $Fe_2P_2O_7$; Thermochemical reduction; Microspheres

1. Introduction

Iron-based compounds are very attractive as electrode materials for rechargeable lithium batteries since they are inexpensive, nontoxic, and environmentally benign. Iron-based compounds have been synthesized in a variety of morphologies, including nanoparticles [1], nanowires [2], nanorods [3], nanotubes [4], and nanoflakes [5]. However, iron-based compounds usually suffer from rapid capacity fading as a result of large volume change during Li conversion reactions [6].

Iron phosphates have been explored as both cathode and anode materials in Li-ion batteries. In particular, $LiFePO_4$ exhibits a theoretical capacity of 170 mA h g^{-1} when operating as a cathode material. On the other hand, iron phosphates such as $FePO_4$ and Fe_3PO_7 typically act as anode materials, and consequently, they are expected to show reaction mechanisms that are different from those of cathodic lithium iron phosphates [7,8]. Recently, Hu et al. reported the synthesis of a $LiFePO_4$ cathode from an $Fe_2P_2O_7$ precursor. Fe and P (having valences of +2 and +5, respectively) were present with a Fe/P molar ratio of 1:1 in both $Fe_2P_2O_7$ and $LiFePO_4$ [9]. However, to the best of our knowledge, the Li electroactivity of $Fe_2P_2O_7$ has not been reported.

Herein, we report for the first time the utilization of $Fe_2P_2O_7$ as an anode material in Li-ion batteries. The synthesis was performed by controlled thermal dehydrogenation and subsequent thermochemical reduction of precursor $FePO_4 \cdot 2H_2O$ microspheres composed of self-assembled nanorods. The as-prepared $Fe_2P_2O_7$ microspheres exhibited higher specific capacity and significantly superior cycling performance characteristics compared to $FePO_4 \cdot 2H_2O$.

2. Experimental procedure

The starting materials were iron(III) chloride ($FeCl_3$, Aldrich, purity 99%), phosphoric acid (H_3PO_4, Aldrich, purity 98%), and sodium sulfate (Na_2SO_4, Aldrich). Aqueous solutions of $FeCl_3$ (150 mL, 0.2 M) and H_3PO_4 (100 mL, 0.3 M) were mixed and vigorously stirred. The resulting solution was added to Na_2SO_4 (10.65 g, 0.3 M) with constant stirring for 30 min and then transferred to a 300-mL Teflon-lined stainless steel autoclave. The autoclave was sealed and heated to 120 °C (heating rate of 10.0 °C min^{-1}) for 1–24 h, after which it was cooled down to room temperature. As a result of this treatment, a $FePO_4 \cdot 2H_2O$ precipitate was obtained. This precipitate

*Corresponding author. Tel.: +82 31 219 2468; fax: +82 31 219 1612.
E-mail address: dwkim@ajou.ac.kr (D.-W. Kim).

0272-8842/$36.00
http://dx.doi.org/10.1016/j.ceramint.2012.05.032

was collected by centrifugation, washed several times with deionized water and ethyl alcohol, and finally dried overnight at 60 °C in a vacuum oven. Then, the as-prepared $FePO_4 \cdot 2H_2O$ precursor was treated at 400 °C for 24 h under flowing hydrogen (300 sccm).

The powder materials obtained were characterized by X-ray diffraction (XRD, Bruker AXS D8, Germany) and scanning electron microscopy (SEM, HITACHI S-4100, Japan). In order to determine the electrochemical behavior of the prepared materials, positive electrodes were fabricated by mixing the powders with Super P carbon black (MMM Carbon, Brussels, Belgium) and a Kynar 2801 binder (PVdF-HFP) in a mass ratio of 70:15:15 and subsequently pasting the mixture on a Cu foil. Swagelok-type cells containing Li metal foil (employed as the anode) and a separator film of Celgard 2400 were assembled and saturated with the liquid electrolyte (1 M $LiPF_6$ in a 1:1 (by volume) mixture of ethylene carbonate and dimethyl carbonate, Techno Semichem Co., Ltd., Korea). The assembled cells were galvanostatically cycled between 0.0 and 2.5 V using an automatic battery cycler (WBCS 3000, WonA-Tech, Korea).

3. Results and discussion

Fig. 1 shows SEM images of the $FePO_4 \cdot 2H_2O$ powder for several hydrothermal reaction times. The concentration of reactants was fixed at 0.12 M in all the cases. Fig. 1a shows the morphology of the powders at the early growth stage (1 h hydrothermal treatment). It can be seen that several hundred nanometer-sized particles were formed initially, and each particle was composed of tiny nanoparticles, as indicated in the inset of Fig. 1a. The XRD patterns for these particles showed an amorphous phase (data not shown). When longer hydrothermal treatments were applied (5–8 h), the particles grew to a size of several micrometers (≈ 3 μm) with spherical morphology, as observed in Fig. 1b and c. Interestingly, the microspheres were constructed of several densely-packed crystalline nanorods with diameters of 30–50 nm and lengths of 200 nm, as shown in the magnified SEM images (insets of Fig. 1b and c). After a prolonged hydrothermal reaction time (24 h), some microspheres grew abnormally to ≈ 15 μm, so a bimodal particle size distribution was observed (Fig. 1d). A possible growth model based on these SEM images is illustrated in Fig. 1e. During the initial stages of the reaction,

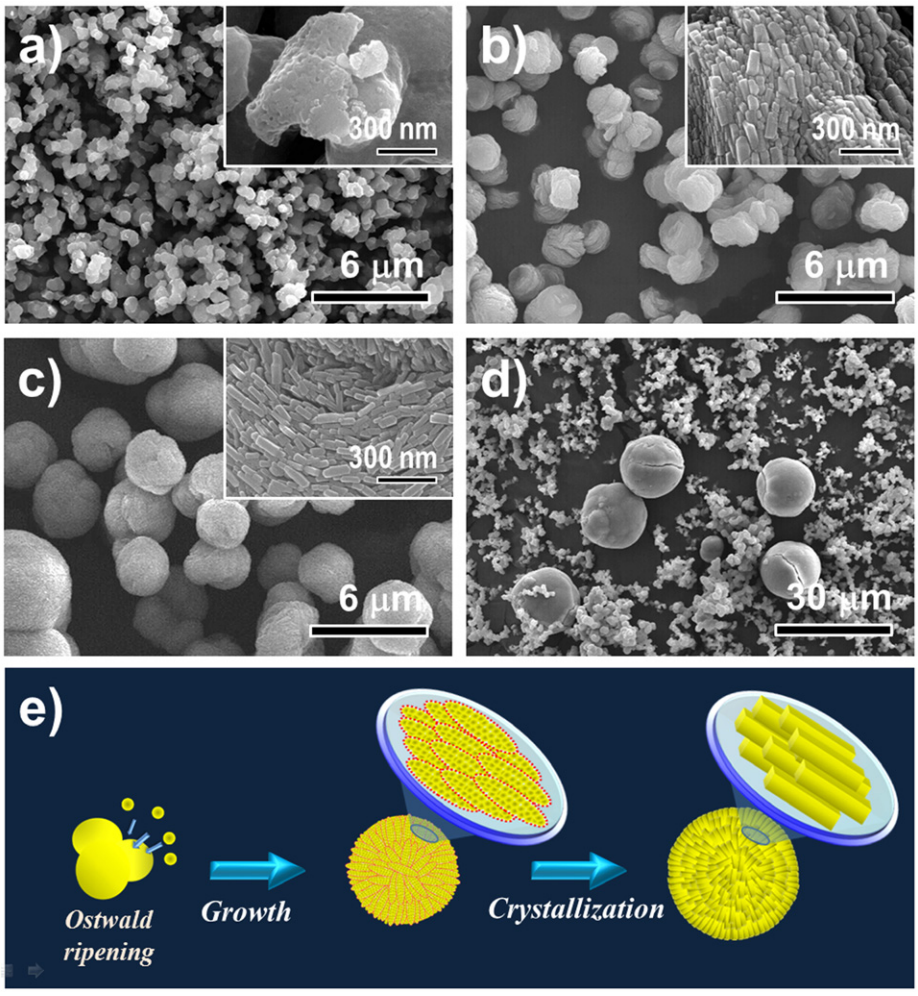

Fig. 1. Typical SEM images of $FePO_4 \cdot 2H_2O$ powders after hydrothermal reaction at 120 °C for (a) 1 h, (b) 5 h, (c) 8 h, and (d) 24 h. Insets in (a–c) show the magnified images of the surface of each particle. (e) Schematic illustration of the morphological evolution.

tiny precipitates coagulated by the Ostwald ripening thereby forming amorphous nanoparticles [10]. Subsequently, further reaction allowed these tiny precipitates to grow forming elongated nanorods through oriented aggregation. These nanostructures finally crystallized generating $FePO_4 \cdot 2H_2O$ microspheres composed of self-assembled nanorods.

Thermogravimetric (TG) analysis of $FePO_4 \cdot 2H_2O$ microspheres (Fig. 2a) revealed an abrupt change in the slope of the weight loss curve at about 200 °C, which could be ascribed to the formation of a tridymite $FePO_4$ phase by dehydration of the as-prepared $FePO_4 \cdot 2H_2O$ [7]. The sharp endothermic peak near this temperature in the differential thermal analysis confirmed the thermal decomposition of $FePO_4 \cdot 2H_2O$.

In order to favor the synthesis of the ferrous salt (e.g., $Fe(II)_2P_2O_7$) versus the $Fe(III)PO_4$ phase, the $FePO_4 \cdot 2H_2O$ precursors were thermochemically reduced at 400 °C under flowing H_2. As described above, a $FePO_4 \cdot 2H_2O$ phase can be prepared after hydrothermal reaction for 8 h (Fig. 2b). This precursor phase was completely transformed to $Fe_2P_2O_7$ after the reduction treatment according to the following reaction:

$$2Fe(III)PO_4 \cdot 2H_2O + H_2 \rightarrow Fe(II)_2P_2O_7 + 5H_2O$$

The divalent metal pyrophosphates $Fe_2P_2O_7$ possess three polymorphs (α, β, and γ). Hoggins et al. found that

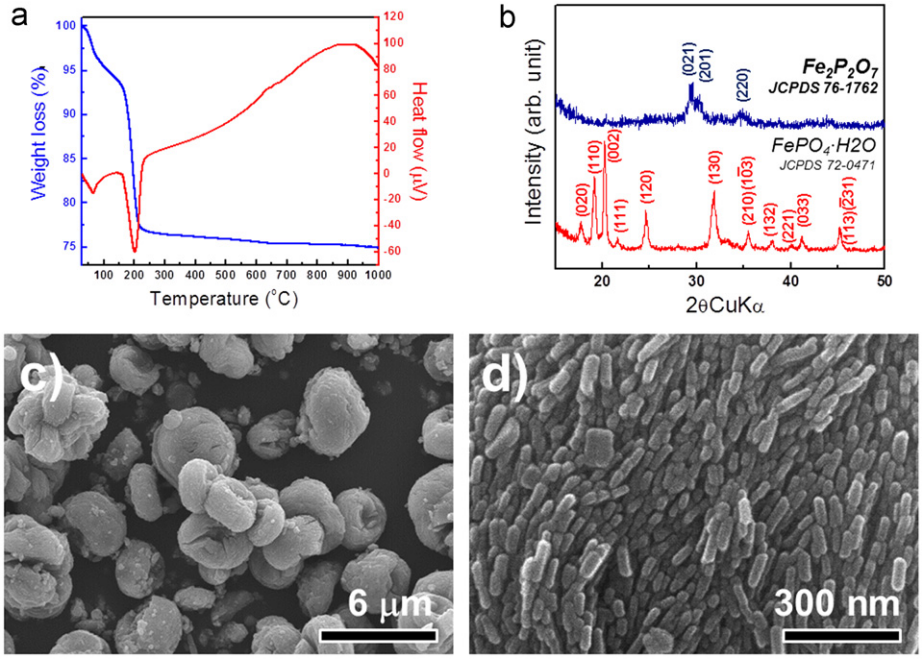

Fig. 2. (a) TGA-DTA curves of the $FePO_4 \cdot 2H_2O$ microspheres under air; (b) XRD patterns of the $FePO_4 \cdot 2H_2O$ and $Fe_2P_2O_7$ microspheres; (c) low- and (d) high-magnification SEM images of the $Fe_2P_2O_7$ microspheres.

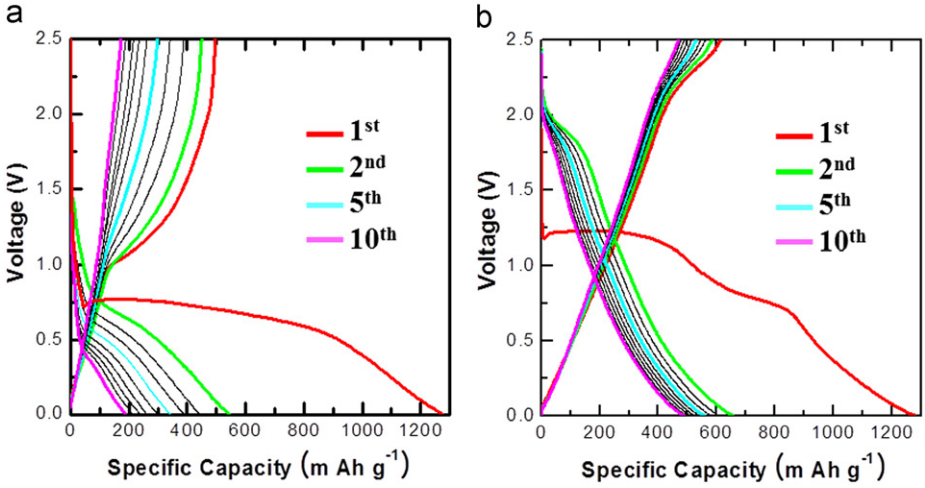

Fig. 3. Galvanostatic discharge/charge voltage profiles of the (a) $FePO_4 \cdot 2H_2O$ and (b) $Fe_2P_2O_7$ electrodes at a rate of 100 mA g^{-1}.

the unit cells of other monoclinic metal pyrophosphates $M_2P_2O_7$ compounds (M = Mn, Cu, Mg, Zn) belonged to the same unconventional $C\bar{1}$ space group. The as-prepared $Fe_2P_2O_7$ crystallizes in the $C\bar{1}$ space group and has the form β-$Fe_2P_2O_7$ in the crystal phase. Actually, β-$Fe_2P_2O_7$ is a triclinic distortion of this form. The Fe octahedron irregularity and the iron in tetrahedral coordination have been previously observed for the Mg–O octahedron, which is isostructural with the β-$Mg_2P_2O_7$ structure [9,11].

Overall, the $FePO_4 \cdot 2H_2O$ precursor showed a spherical morphology, although each microsphere was shrunken and partially crushed (Fig. 2c). The magnified SEM image of the surface of $Fe_2P_2O_7$ in Fig. 2d indicated a microsphere constructed of nanorods, which were shortened (≈ 100 nm) as a result of prolonged reduction. These morphological changes were previously ascribed to volume changes produced by phase conversion and dehydration processes during the reduction process [6].

The galvanostatic cycling characteristics of both $FePO_4 \cdot 2H_2O$ and $Fe_2P_2O_7$ microspheres in the configuration of product/Li half-cells were investigated over the range 0.0–2.5 V at 100 mA g^{-1} for 10 cycles (Fig. 3). Fig. 3a shows the voltage-specific capacity curve of the $FePO_4 \cdot 2H_2O$ nanorods/spheres, which showed first discharge and charge capacities of 1273 and 495 mA h g^{-1}, respectively. However, the reversible capacity faded drastically to 187 mA h g^{-1} after 10 cycles, which is in good agreement with previous reports [7]. On the other hand, the first discharge and charge capacities of $Fe_2P_2O_7$ were 1281 and 613 mA h g^{-1}, respectively, and a high reversible capacity of ≈ 500 mA h g^{-1} was obtained after 10 cycles, which is higher than that of commercial, graphite-based anodes. The inferior cycling performance of $FePO_4 \cdot 2H_2O$ might be attributed to the existence of water in the crystal structure and the dense assembly of nanorods in each microsphere thereby hindering the permeability of the electrolyte. $Fe_2P_2O_7$ microspheres were prepared through the complete dehydration process during thermochemical reduction. In addition, each $Fe_2P_2O_7$ microsphere showed a relatively open, porous structure comprising loosely packed nanorods. Therefore, the superior capacity retention of the $Fe_2P_2O_7$ microspheres resulted from the better accommodation of the liquid electrolyte within the lattice, which enhanced Li-ion transfer [6,12,13].

4. Conclusions

In summary, we report herein the synthesis of $Fe_2P_2O_7$ microspheres composed of assembled nanorods via simple thermochemical reduction of hydrothermally-prepared $FePO_4 \cdot 2H_2O$ precursor microspheres. The morphology and crystallinity of the $FePO_4 \cdot 2H_2O$ microspheres can be easily controlled by adjusting the length of the hydrothermal treatment. The $Fe_2P_2O_7$ microspheres, with their open porous structure, exhibited a better lithium storage capacity upon cycling than $FePO_4 \cdot 2H_2O$ microspheres. These results can be explained in terms of improved electrolyte permeability and Li-ion transfer characteristics. Therefore, these prepared $Fe_2P_2O_7$ microspheres may be potential host materials for high-energy Li-ion batteries.

Acknowledgments

This work was supported by the National Research Foundation of Korea (NRF) grant funded by the Korea government (MEST) (nos. 2011–0005776 and 2011–0030745).

References

[1] X.L Wu, Y.G. Guo, L.J. Wan, C.W. Hu, α-Fe_2O_3 nanostructures: inorganic salt-controlled synthesis and their electrochemical performance toward lithium storage, J. Phys. Chem. C 112 (2008) 16824.
[2] Q. Han, Z. Liu, Y. Xu, Z. Chen, T. Wang, H. Zhang, Growth and Properties of Single Crystalline γ-Fe_2O_3 Nanowires, J. Phys. Chem. C 111 (2007) 5034.
[3] C. Wu, P. Yin, X. Zhu, C. OuYang, Y. Xie, Synthesis of hematite (α-Fe_2O_3) nanorods: diameter-size and shape effects on their applications in magnetism, lithium ion battery, and gas sensors, J. Phys. Chem. B 110 (2006) 17806.
[4] J. Chen, L. Xu, W. Li, X. Guo, α-Fe_2O_3 nanotubes in gas sensor and lithium-ion battery applications, Adv. Mater. 17 (2005) 582.
[5] M.V. Reddy, T. Yu, C.H. Sow, Z.X. Shen, C.T. Lim, G.V. Rao, B.V.R. Chowdari, α-Fe_2O_3 nanoflakes as an anode material for Li-ion batteries, Adv. Funct. Mater. 17 (2007) 2792.
[6] G.H. Lee, J.G. Park, Y.M. Sung, K.Y. Chung, W.I. Cho, D.W. Kim, Enhanced cycling performance of an Fe/Fe_3O_4 nanocomposite electrode for lithium-ion batteries, Nanotechnology 20 (2009) 295205.
[7] D. Son, E. Kim, T.G. Kim, M.G. Kim, J. Cho, B. Park, Nanoparticle iron-phosphate anode material for Li battery, Appl. Phys. Lett. 85 (2004) 5875.
[8] Y.S. Hong, Y.J. Park, K.S. Ryu, S.H. Chang, Crystalline Fe_3PO_7 as an anode material for lithium secondary batteries, Solid State Ionics 156 (2003) 27.
[9] G.R. Hu, Z.W. Xiao, Z.D. Peng, K. Du, X.R. Deng, Preparation of $LiFePO_4$ for lithium ion battery using $Fe_2P_2O_7$ as precursor, J. Cent. South Univ. Technol. 15 (2008) 531.
[10] R. Boistelle, J.P. Astier, Crystallization mechanisms in solution, J. Crystal Growth 90 (1988) 14.
[11] J.T. Hoggins, J.S. Swinnea, H. Steinfink, Crystal structure of $Fe_2P_2O_7$, J. Solid State Chem. 47 (1983) 278.
[12] S.H. Lee, S.D. Seo, Y.H. Jin, H.W. Shim, D.W. Kim, A graphite foil electrode covered with electrochemically exfoliated graphene nanosheets, Electrochem. Commun. 12 (2010) 1419.
[13] H.W. Shim, D.K. Lee, I.S. Cho, K.S. Hong, D.W. Kim, Facile hydrothermal synthesis of porous TiO_2 nanowire electrodes with high-rate capability for Li ion batteries, Nanotechnology 21 (2010) 255706.